2018-09

On the edge of exceptional preservation: insights into the role of redox state in Burgess Shale-type taphonomic windows from the Mural Formation, Alberta, Canada

Sperling, EA

10.1042/ETLS20170163
Emerging Topics in Life Sciences
Portland Press Ltd.

On the edge of exceptional preservation: insights into the role of redox state in Burgess Shale-type taphonomic windows from the Mural Formation, Alberta, Canada

Erik A. Sperling[1*], Uwe Balthasar[2], Christian B. Skovsted[3]

[1] Department of Geological Sciences, Stanford University, Stanford, CA, USA 94305

[2] School of Geography, Earth and Environmental Sciences, University of Plymouth, PL4 8AA, Plymouth, United Kingdom

[3] Department of Palaeobiology, Swedish Museum of Natural History, Box 50007, SE-104 05 Stockholm, Sweden

* Corresponding author:

Dr. Erik A. Sperling
Department of Geological Sciences
Stanford University
Stanford, CA, USA 94305
650-736-0852 (v)
esper@stanford.edu

Keywords: Cambrian; Mural Formation; Burgess Shale-type preservation; Oxygen; taphonomy; iron reduction

Abstract

Animals originated in the Neoproterozoic and 'exploded' into the fossil record in the Cambrian. The Cambrian also represents a high point in the animal fossil record for the preservation of soft tissues that are normally degraded. Specifically, fossils from Burgess Shale-type (BST) preservational windows give paleontologists an unparalleled view into early animal evolution. Why this time interval hosts such exceptional preservation, and why this preservational window declines in the early Paleozoic, have been long-standing questions. Anoxic conditions have been hypothesized to play a role in BST preservation, but recent geochemical investigations of these deposits have reached contradictory results with respect to the redox state of overlying bottom waters. Here, we report a multi-proxy geochemical study of the Lower Cambrian Mural Formation, Alberta, Canada. At the type section, the Mural Formation preserves rare recalcitrant organic tissues in shales that were deposited near storm wave-base (a Tier III deposit; the worst level of soft-tissue preservation). The geochemical signature of this section shows little to no evidence of anoxic conditions, in contrast to published multi-proxy studies of more celebrated Tier I and II deposits. These data help confirm that 'decay limited' BST biotas were deposited in more oxygenated conditions, and support a role for anoxic conditions in BST preservation. Finally, we discuss the role of iron reduction in BST preservation, including the formation of iron-rich clays and inducement of sealing seafloor carbonate cements. As oceans and sediment columns became more oxygenated and more sulfidic through the early Paleozoic, these geochemical changes may have helped close the BST taphonomic window.

Introduction

The Cambrian radiation of animal life represents the appearance of nearly every major animal phylum in the fossil record within a geologically rapid span of ~25 million years. The rapid increase in animal diversity and disparity is apparent in multiple records including the normal shelly fossil record (e.g. brachiopods, trilobites; (1)), the trace fossil record (2–4), phosphatized small shelly fossils (5–7) and small carbonaceous fossils (SCFs; (8,9)). The most celebrated archive of this event, though, is from Burgess Shale-type (BST) deposits, where primary organic tissues are preserved as thin carbonaceous films (see (10) for definitions). Critically, these lagerstätten preserve the soft parts of animals, and while the communities do not preserve a completely unbiased snapshot of early Cambrian life (for instance, size; (11)), they do provide our best glimpse of early metazoan ecosystems (12–15). Most important, by preserving most or all characters of an organism, fossils from BST biotas have been critical in understanding the polarity and order of morphological character evolution within each individual phylum (16).

The question of how organisms can escape the decay process, and why these BST lagerstätten appears to be concentrated in the Cambrian period—even after accounting for factors like rock outcrop area (17,18)—has long intrigued geologists. It was recognized early on that low oxygen levels (or complete anoxia) might play a prominent role in reducing decay. Actualistic decay experiments, however, established that decay under anoxic conditions (at least in the presence of normal marine sulfate levels) can still proceed rapidly (19,20). For soft-bodied deposits in general, then, anoxia mainly serves to 1) prevent scavenging, which would otherwise destroy carcasses (21), and 2) help induce the precipitation of authigenic minerals, which are involved in most exceptionally preserved deposits (22). In the most recent review of BST

preservation (10), the window for abundant and exquisite BST fossil preservation is hypothesized to occur in a 'goldilocks' zone near where the chemocline (the point in the water column at which no oxygen remains) intersects the seafloor. At seafloor depths well below the chemocline, the setting is 'supply limited' in that animals cannot live in anoxic conditions, and carcasses simply cannot be supplied to these preservational settings through transport. Only preservation of nektonic/planktonic organisms falling through the water column could potentially occur. Conversely, at seafloor depths well above the chemocline, the setting is 'decay limited' (preservation limited) in that aerobic degradation and bioturbating organisms quickly destroy carcasses. Gaines (10) directly related the quality of preservation and species-level diversity of BST biotas to the position of these deposits along the spectrum from 'supply limited' to 'decay limited'. The most spectacular deposits, such as the Burgess Shale and Chengjiang (Tier 1), are hypothesized to occur in the window where there is sufficient transport energy to carry soft-bodied benthic organisms across the chemocline into anoxic waters. Tier II deposits such as Kaili, Marjum and Spence lack sufficient transport energy or have source communities too far up-slope above the chemocline, and so it is dominantly hydrodynamically light organisms (e.g. algae) or dead carcasses that can be carried to the zone of exceptional preservation. Conversely, the labile tissues of organisms living in-situ in these up-slope communities are only rarely preserved due to the prevalence of more oxygenated conditions. Thus at different points along a water-depth transect these Tier II deposits are both supply- and decay-limited. Tier III deposits such as Latham or Indian Springs are hypothesized to have been deposited near storm wave-base in relatively oxygenated conditions, and soft tissues are almost completely decomposed. Or in another sense, only the most recalcitrant tissues are preserved (e.g., (23)). These Tier III sites are consequently the most 'decay limited' in this classification scheme.

This hypothesized relationship between BST preservation and the chemocline (10) has mainly been developed on the basis of sedimentological and ichnological data (e.g., (24)). To test this framework, in recent years geochemists have applied several tools to the question, most notably iron speciation analysis and the study of redox-sensitive trace metal concentrations. Both of these proxies rely on identifying enrichments of specific phases or elements (that are known to be incorporated into sediments under reducing conditions) relative to average crustal values or empirically determined shale baselines. Iron speciation tracks the ratio of total iron (FeT) to highly reactive iron phases (FeHR; iron in pyrite plus those iron phases reactive to sulfide on early diagenetic timescales, including iron oxides, iron carbonates and magnetite). In the modern ocean, samples deposited beneath an oxygenated water column have FeHR/FeT < 0.38 (25,26). Samples deposited beneath an anoxic water column generally have ratios > 0.38, although rapid deposition, for instance in turbidites, can mute enrichments (the lowest modern anoxic samples have ratios as low as 0.20; (25,27)). Critically, this proxy can also distinguish different types of anoxic water columns: between anoxic and ferruginous water columns (those with free ferrous iron, or more specifically not enough sulfide production to titrate available reactive iron) and anoxic and euxinic water columns (with free sulfide). This is accomplished by examining the proportion of reactive iron that has been pyritized (FeP; represents iron in pyrite). Generally, anoxic samples with FeP/FeHR > 0.7-0.8 are interpreted as euxinic, with ratios below this interpreted as ferruginous (26). As discussed below, whether a water column was ferruginous versus euxinic has important implications for interpreting trace metal patterns, and, perhaps, BST preservation itself.

Analysis of redox-sensitive trace metal concentrations relies on the observation that these elements (such as molybdenum, uranium, vanadium or chromium) are generally soluble in

oxygenated water columns, and become insoluble and form complexes with organic matter, sulfides or other mineral phases upon reduction in suboxic (only trace amounts of oxygen present; ~ 0.1 mL/L) or anoxic (zero oxygen) water columns (28). Such authigenic metal enrichments are identifiable by comparing concentrations in a given shale sample against baselines meant to represent the background detrital input, such as world average shale (29) or average upper continental crust (30). Concentrations above these baselines would point towards authigenic enrichment, and by inference, a reducing water column. Like with iron speciation, rapid deposition will result in less time for authigenic enrichments to accumulate.

The sequestration pathways for each element are unique, with different reducing conditions and the presence/absence of sulfide having large effects on the level of enrichment. For instance, sulfide levels > 11μM are required for the quantitative switch from molybdate anion to tetrathiomolybdate, which increases particle reactivity and hence the removal of Mo from the water column into the sediment (31,32). Vanadium does not require sulfidic conditions for initial reduction, but also undergoes a second reduction step in the presence of significant sulfide levels (33), and the presence of large sedimentary V enrichments may require sulfide. Historically, most of the research on authigenic metal enrichment has focused on modern systems or Mesozoic Ocean Anoxic Events, both of which are characterized by water columns and sediments that were generally sulfidic when anoxic. However, ferruginous conditions are increasingly being identified throughout pre-Mesozoic oceans (26,34–36), and recent debate has focused on expected metal enrichments under such conditions (27,37–40). Although this debate remains open with respect to the exact magnitude of enrichment expected, studies have agreed that redox-sensitive metal enrichments will be relatively muted in ancient ferruginous settings. Further complicating the picture, two elements whose enrichment does not depend on the strict

154 presence of sulfide—vanadium and chromium—are the redox-sensitive metals most influenced
155 by variations in the detrital fraction, making the detection of muted enrichments difficult (28,41).
156
157 **Redox studies of BST deposits**
158 Analyses using iron speciation and some studies of redox-sensitive metal concentrations
159 have provided contrasting interpretations of redox state during deposition of Burgess Shale-type
160 deposits. Consistent with a role for anoxia in the preservational model, iron speciation analyses
161 of the Series 3 Wheeler Shale, Utah, have indicated a mixture of ferruginous and oxic conditions
162 ((35,42); although note that no data to date has been presented in stratigraphic or paleontological
163 context). An iron speciation and trace metal abundance investigation of the Series 2 Chengjiang
164 lagerstätte, South China, revealed euxinic conditions stratigraphically beneath the exceptionally
165 preserved deposits, followed by the development of more 'equivocal' conditions in the zone of
166 exceptional preservation (43). Specifically, FeP/FeHR ratios were <0.7, and FeHR/FeT ratios
167 were between 0.2 and 0.38, which in combination with low Mo concentration and in the context
168 of the turbiditic setting, could indicate either an oxic or ferruginous water column (43,44).
169 Nitrogen isotopes were also investigated in these Chengjiang cores, and showed a more readily
170 interpretable signal. Hammarlund et al. (43) suggested, based on positive nitrogen isotope values,
171 that the water column was strongly denitrifying (similar to the cores of modern Oxygen
172 Minimum Zones; OMZs) above the zone of exceptional preservation. Overall, these data point
173 towards 'suboxic' to anoxic (but non-sulfidic) conditions during deposition of the Chengjiang
174 BST deposits. Echoing these results, a detailed multi-proxy study of the Series 2 Sirius Passet
175 deposit in North Greenland reported transiently anoxic (ferruginous) conditions during the
176 interval of highest soft-bodied fossil abundance and diversity (45).

In contrast, trace metal data from these and other BST deposits have been interpreted as indicative of oxygenated conditions at the seafloor. Near-crustal levels of redox-sensitive metals (e.g. Mo, U, V, Cr) have been found in the Burgess Shale itself (46), Chengjiang (42,43; though higher abundances were found in the lower Maotianshan Shale), Sirius Passet (47), Emu Bay lagerstätte in South Australia (48), the Rockslide Formation in northwestern Canada (49), the Wheeler and Spence shales in Utah (44) and the Indian Springs lagerstätte, Nevada (50). These relatively low enrichments have generally been interpreted as representing a purely detrital trace metal source and an oxygenated water column. Consequently, it has also been inferred that anoxia did not play a role (or was not required) for BST preservation. In some cases, the robustness of these trace metal signals has been questioned because some deposits (such as the Burgess Shale and Sirius Passet) have experienced considerable metamorphism (24). However, given the consistent and widespread pattern in deposits with lower metamorphic grade, this is probably a primary depositional signature. But while likely primary, the common interpretative paradigm that low redox-sensitive trace metal contents indicate oxygenated conditions (e.g. Jones and Manning ref. (51)) was developed prior to our current understanding that anoxic but non-sulfidic (ferruginous) water columns—with low trace metal enrichments compared to euxinic systems—are common in the geological record. Given this new framework, these published trace metal data provide no evidence for euxinic conditions, but they are also consistent with the muted trace metal enrichments predicted for shale deposited under a ferruginous water column. Thus the role of redox state in BST preservation remains controversial.

The Mural Formation: a test case

The Lower Cambrian (Series 2) Mural Formation, exposed in the southern Canadian Cordillera (Fig. 1), offers an opportunity to refine our understanding of the role of redox state in BST preservation. In terms of preservation, the Mural Formation contains elements of BST soft-bodied preservation in one known locality near Mumm Peak (Fig. 1; Fig. 2D, E), but compared to Tier I and II biotas such as the Burgess Shale, Sirius Passet, Emu Bay, or Chengjiang, it is by no means 'exceptional' in terms of abundance or preservational fidelity. In essence, it preserves recalcitrant cuticles rather than fine morphologies. Also in contrast to most BST deposits that were deposited well beneath storm wave-base (10), the Mural Formation shows evidence of storm activity in stratigraphic proximity to the beds with exceptional preservation. The Mural Formation therefore represents an end-member of BST preservation: perhaps deposited in slightly shallower water, and with soft-part preservation not seen in standard shelly faunas, but not as exceptional as the deservedly more famous BST deposits. In the classification of Gaines (10) this is a 'Tier 3' BST deposit (the worst level of fossil preservation). The goal of this study is to conduct a multi-proxy sedimentary geochemical study of the BST-preservation interval in the Mural Formation—the first such study of a Tier 3 deposit—and compare the results against data obtained from other BST deposits worldwide. Overall this work provides data from a preservational end-member on the role of oxygen in BST taphonomy and an important consistency test of existing hypotheses: if anoxia plays a central role in exceptional BST preservation, we would predict a more oxygenated signal in the Mural Formation than the investigated Tier I and II deposits.

Geologic Background

The Mural Formation was deposited during the early Cambrian Sauk transgression on the western Laurentian margin (52,53), and sits above the ~300-1700 meter thick shallow-marine siliciclastics of the McNaughton Formation (54,55). The McNaughton is generally thought to represent the rift-to-post-rift transition on the Laurentian margin (56,57) although continued syn-sedimentary faulting continued through the mid-Cambrian to the north. The Mural Formation is part of a broadly contiguous stratigraphic package spanning the *Nevadella – Bonnia/Olenellus* trilobite zones (Series 2; Waucoban) that stretches from Mexico to Yukon, Canada (52). This package consists of an upper and lower carbonate composed of ooid grainstone shoals and archaeocyath bioherms, separated by a medial shale/siltstone (Fig. 3).

The Mural Formation has been the subject of paleontological investigation for more than a century (primarily at its type section near Mumm Peak, Jasper National Park, the focus of study here), and workers have described an abundant shelly fauna including trilobites and obollelid and linguliform brachiopods (58–63). Two known levels have also yielded soft-part preservation (Fig. 3), the '*Lingulosacculus* quarry' that preserves soft-shelled brachiopods (64) (Fig. 2E), and the 'waterfall quarry' level which contains as-yet undescribed vetulicolians, palaeoscolecid worms, and anomalocarid appendages (Fig. 2D). These soft-bodied preservation levels are located in grey, laminated shales between packages of shale containing beds and lenses of detrital carbonates, sometimes comprised of fossil hash. Whether these storm beds represent a shallowing into storm wave base during sea-level change (i.e. parasequences) or occasional storm beds at a constant depth could not be determined, but in either case this represents a proximity to wave base not seen in Type I and II BST deposits (10). The Mural Formation does not display bioturbation through the medial shale.

Materials and Methods

27 shale samples were collected from the Mural Formation, all from the medial shale at the type section, and crushed in a tungsten carbide shatterbox. Total organic carbon (TOC) weight percent was analyzed on decalcified residue on a Carlo-Erba NA 1500 Elemental Analyzer. Weight percent iron in pyrite (FeP) was quantified using the chromium reducible sulfur method of Canfield et al. (65), and iron present in iron oxides, iron carbonates and magnetite was quantified using the sequential extraction method of Poulton and Canfield (66). Precision estimates for these methods can be found in the supplementary materials of (35,40). Major, minor and trace element concentrations were analyzed by Bureau Veritas, Ltd., using ICP-MS/ICP-OES following multi-acid digestion. Aliquots of the USGS shale standards SBC-1 and SGR-1 were sent blind along with samples, and results were consistent with published values.

Results and discussion

All geochemical results are plotted on Figure 3 and reported in the Supplementary Information. Total organic carbon (TOC) weight percents in the Mural Formation are relatively low, at 0.14 ± 0.03 (one standard deviation). This probably rules out very high original sedimentary TOC values (as this signature can be retained even in the face of metamorphism, e.g., (67), but as these are outcrop samples from a region that has experienced prehnite-pumpellyite grade (CAI of 3-5) metamorphism (68), the original TOC-richness is unknown and certainly higher. Redox-sensitive trace metal contents are uniformly low and around crustal/average shale values. Specifically, Mo contents are all < 1 ppm, U contents are 2.6 ± 0.4 ppm, and V contents are 88 ± 8 ppm. As aluminum, a conservative tracer of detrital input, is also

near or even slightly elevated compared to average shale values (9.4 ± 0.5 weight percent), the low redox-sensitive trace metal contents in the Mural cannot be explained by dilution by carbonates or other non-clastic material. Trace metal data are plotted in Figure 3 as Enrichment Factors (EF), which is a method of accounting for the expected detrital metal input based on observed levels of a biogeochemically conservative element such as aluminum (discussed in (28)). Values >>1 would indicate authigenic enrichment (due to reducing conditions). Values around 1 generally indicate the operation of purely detrital processes and oxic conditions, however since there is so much possible variability in detrital input (41), and substantial authigenic metal enrichments might also not develop during rapid sedimentation, recognizing whether there have actually been slight enrichments or depletions is difficult to tell. The Mural Formation data unfortunately falls in this zone. Thus, like many other BST deposits investigated to date, the Mural Formation trace metal data rule out euxinic conditions but are consistent with either an oxic (no enrichment) or ferruginous (possibly muted enrichment) water column during deposition.

The iron geochemistry of the Mural Formation, though, differs from that of investigated BST deposits. FeHR/FeT values are low (0.17 ± 0.04), with all of the values being well below the 0.38 ratio usually taken as indicative of an anoxic water column. The most straightforward explanation of these data is oxic deposition. However, it has been recognized that 1) fingerprinting anoxia is generally more straightforward than oxic conditions (37,69) and 2) there are a number of factors that can result in low FeHR enrichment (rapid deposition and source area effects) or drive FeHR/FeT values lower (metamorphism). Regarding rapid deposition, the medial shale does not have consistent sedimentological indicators of such processes, although it should be noted that obvious sedimentary structures are difficult to see in outcrop. There is

291 evidence for event-driven sedimentation in a relatively thick sandstone marker bed right above
292 the exceptionally preserved interval. Considering that almost all BST deposits involve event-
293 based sedimentation (10), more detailed sedimentological and petrographic study of the Mural
294 Formation may reveal additional evidence of these processes. Nonetheless, the observed
295 FeHR/FeT values are still generally lower than the lowest 0.2 ratio recognized in the modern
296 ocean for anoxic turbidites (27), suggesting a most parsimonious interpretation of oxic
297 conditions even with respect to this caveat. Second, in some cases there may not be an
298 appropriate source of detrital iron available to be shuttled into the anoxic basin, and it is this
299 shuttle that ultimately generates the iron enrichments this proxy targets (discussed in (69)).
300 However, such settings are relatively rare, and stratigraphically underlying anoxic
301 Neoproterozoic strata exhibit obvious iron enrichments (36). Perhaps the most important
302 consideration for the Mural is that highly reactive iron can be converted to poorly reactive iron
303 during metamorphism, removing the evidence for anoxic sedimentation ((26,70). Fortunately,
304 total iron (relative to aluminum) is also generally enriched by the iron shuttle under anoxic water
305 columns (71,72), and this ratio is not as strongly affected by metamorphism. With the exception
306 of one sample (interestingly, at the level of the *Lingulosacculus* quarry; Fig. 3), the Fe/Al values
307 (0.48 ± 0.11) are exactly within the range expected of oxic sediments (72). In summary, although
308 we cannot unambiguously rule out anoxic conditions, we can state 1) the only possible anoxic
309 signal—in just one of multiple proxies—occurs at one of the soft-bodied preservation levels, and
310 2) all other available evidence points towards the presence of at least some oxygen in the water
311 column (or more precisely, provides no evidence for anoxia).
312 The Mural Formation thus preserves elements of BST biotas and has no evidence for
313 anoxia. Although seemingly paradoxical, we argue this provides strong evidence for the role of

anoxic or periodically anoxic conditions in BST preservation. Put simply, the preservation in the Mural Formation is nowhere near that in the celebrated BST deposits. There is no exquisite, high-fidelity preservation of nervous systems, eyes, gut details, gills, etc. as in other deposits (73–76). The fossils preserved in the Mural Formation at Mumm Peak are the recalcitrant end-members of BST preservation: soft-shelled brachiopods (64), anomalocarid appendages, etc. Exceptionally preserved fossils in the Mural Formation are also rare and low-diversity; despite extensive quarrying during our fieldwork, we did not uncover new taxa that had not been found by previous field parties. Core

When comparing between BST deposits, it is worth noting that the overall differences in redox state may have been slight. For instance, the Mural is not extensively burrowed, suggesting the water column was not fully oxygenated. And some of the other more spectacular BST deposits may have been deposited in conditions that rapidly alternated between dysoxic and anoxic/ferruginous conditions, with the chemocline established perhaps only slight above the sediment-water interface (24). However, even considering the known difficulty of tracking low-oxygen conditions with available geochemical proxies (77), it is apparent that exceptional BST deposits (Tier 1 and 2) have a much greater prevalence of anoxic iron speciation signatures and/or total iron enrichments, minor but observable trace metal enrichments, and positive nitrogen isotope values (35,42,43,45) than the Mural Formation. In other words, there is now geochemical evidence suggesting both the Mural Formation and the transition between the upper Maotianshan Shale and Yuanshan Member 3 in the Chengjiang deposit (43) were more oxygenated and ‘decay limited’ than Tier I and II deposits. This confirms previous analyses based on detailed sedimentological and ichnological studies that preservation in BST deposits was facilitated by anoxic conditions (24).

Towards a refined geochemical model

Moving forward, it is clear that anoxia was likely involved in preserving BST fossils, but it is also clear from both sedimentological/ichnological approaches (24,78,79) and multi-proxy geochemical studies (43,45) that these deposits were near the edge of the chemocline, with often-times rapid fluctuations into low-oxygen (suboxic/dysoxic) conditions. Tracking low oxygen levels is difficult with our current geochemical toolkit (77), and further, the ecological/oceanographic timescales that matter for organismal habitat viability and fossil preservation often differ from the integrated longer-term geochemical signals studied in hand samples collected by geochemists (27). Indeed, no published multi-proxy BST dataset is completely unambiguous; such ambiguity may actually be a hallmark of very low-oxygen or fluctuating oxic/anoxic systems. In light of this, further gains in understanding of the role of redox conditions will require new approaches. These may include increased efforts to obtain unoxidized drill cores (packsack or 'winky' drills may offer an alternative to a full drill rig; e.g., (80)), and moving from standard bulk-rock geochemistry (such as in this study) to increased micron- and phase-specific interrogation of the geochemical signal, especially in more metamorphosed deposits. Shale-based proxies that can unambiguously resolve oxygenated conditions would also be a major step forward.

Most important, geochemical studies should strive towards a multi-proxy approach incorporating as many sources of data as possible, but especially pairing redox-sensitive trace metal analysis with iron speciation. The recognition that water columns were commonly ferruginous (non-euxinic) during this time interval will often make interpretation of trace metal data more difficult. Low Mo abundances are helpful in ruling out fully euxinic water columns

(81,82), but in the absence of iron speciation data (the best available method for fingerprinting anoxic but non-euxinic conditions), low concentrations of elements like U, V, and Cr are inconclusive as they could indicate either oxic or ferruginous conditions. Like the Mural Formation, some other 'Tier 3' lagerstätte such as Indian Springs might have been deposited under an oxic water column (50), but this cannot be determined from trace metal data alone. A further issue lies in choosing baseline values. Many studies compare redox-sensitive data to the interpretive scheme of Jones and Manning (51). This study was groundbreaking in its time (especially the cross-validation approach), but current consensus is that the scheme is optimistic in its true ability to detect such subtle redox shifts. Redox-sensitive trace metal behavior in sediments and the water column is complicated, and many of the Jones and Manning proxies (e.g. V/(V + Ni), Ni/Co or V/Cr) take two elements, each with incompletely understood redox properties and perhaps different detrital influences, and combine them together. The sum here is likely less than the parts. In light of this, we propose abandoning the Jones and Manning framework. Nuanced understanding of redox patterns with trace metals remains possible, but this should come through careful comparative study of metal data as single-element enrichment factors or metal/aluminum ratios (while paying heed to possible variation in detrital inputs (41)) and with respect to more modern chemical oceanographic studies.

How exactly anoxic (or fluctuating anoxic-to-dysoxic) conditions directly impacted BST preservation remains unclear. On the one hand, anoxia is a necessary but insufficient prerequisite for BST preservation by eliminating scavenging (10,19,21). Early calcium carbonate cementation and low oceanic sulfate levels may have been equally important in sealing beds from oxidant delivery and reducing microbial decay (83). Beyond simply considering 'anoxia,' it may actually be the specific flavors of anoxia in the sediment and water column that are

383 important in controlling preservation. Specifically, ‘suboxic’ microbial processes such as iron
384 and manganese reduction dramatically increase alkalinity relative to dissolved inorganic carbon
385 (DIC) and thus raise the calcium carbonate saturation state of porewaters. In contrast, sulfate
386 reduction increases alkalinity ~equal to DIC, and moves saturation state along lines of roughly
387 equal values (Ω) (84). Enhanced iron reduction in Cambrian sediments could therefore have
388 helped induce precipitation of the observed BST seafloor cements critical for ‘sealing’ carcasses
389 in the sediment. It is worth noting here that many, but not all, of the BST cement layers carry a
390 dominant seawater (rather than microbial) carbon isotope signature (83). However a seawater
391 carbon signature can also be found in other carbonate precipitates believed to be triggered by
392 ‘suboxic’ microbial metabolisms (84). Essentially, a dominantly seawater carbon isotope
393 signature does not negate a role for iron reduction, but rather suggests that relatively little
394 microbial respiratory work was required to tip the scales and induce precipitation (84).
395 The fact that there was abundant iron reduction relative to sulfate reduction during early
396 diagenesis in BST deposits has recently been demonstrated by clay mineralogy studies. A recent
397 investigation of 19 Cambrian sedimentary successions on four continents found that BST
398 deposits were highly correlated with the presence of iron-rich clay minerals (berthierine and
399 chamosite) compared to deposits only containing shelly fossils (85). These clays form during
400 early diagenesis by the transformation of detrital clays in the presence of elevated pore-water
401 Fe^{2+}. The exact role of these clays in preservation is unclear, specifically whether they are simply
402 a symptom of some other factor important in BST preservational pathways, or a cause (86,87).
403 Certainly, clays appear to function as anti-microbial agents in decay experiments (88), but the
404 action of iron-rich clays is not significantly different from precursors like kaolinite, and the
405 timescale for the formation of berthierine and chamosite is longer than the timescale required for

labile tissue preservation. In any case, considering that pore-water Fe^{2+} will not accumulate in the presence of sulfide (89), it is significant that anoxic Cambrian water columns *and* sediments appear to have had relatively low sulfide-generating potential (35). Thus, a transition in the uppermost sediment column away from extensive iron reduction, and towards sulfate reduction (such as we see in modern OMZs) over the early Phanerozoic may have played multiple geochemical roles in the disappearance of BST preservation. In this view, a transition towards more oxygenated oceans with time may have been important (18), but this alone would be too simplistic; the relative rates of iron versus sulfate reduction matter too. In other words, as oxygen and sulfate levels rose through the Paleozoic (90,91), changes in sediments and water columns towards either more oxic or more sulfidic conditions may have inhibited BST preservational pathways. Most likely, the Burgess Shale-type taphonomic window was propped open by a 'perfect storm' of geochemical parameters in the Cambrian ocean (18,83,86,92).

Summary Points

- Poor preservation in Burgess Shale-type deposits is linked to relatively more oxygenated conditions, suggesting anoxia likely played a role in the most exceptionally preserved deposits.
- The relative dominance of iron reduction compared to sulfate reduction in Cambrian sediments and water columns may have played a key role in factors required for Burgess Shale-type preservation.

Acknowledgements

We thank Una Farrell, Austin Miller, David Mucciarone and Douglas Turner for lab assistance, Jen Wasylyk at Parks Canada for permitting and logistical help, Jakob Vinther for field assistance, Richard Stockey and Ross Anderson helpful discussion, and Bob Gaines and an anonymous reviewer for formal comments. We thank Yellowhead helicopters for safe flying. We gratefully acknowledge support by the National Geographic Society's Global Exploration Fund - Northern Europe GEFNE113-14.

Figure 1- A, B: Geographic position of the Mural Formation section studied here. C: Geological map of the study region, after GSC Map 1499A (93) and modified from (62).

Figure 2- Sedimentology and paleontology of the medial shale/siltstone of the Mural Formation near Mumm Peak. A: Unlike exquisitely preserved Tier I and II BST deposits, the medial shale contains beds and lenses of detrital carbonate with indications of wave or current activity, such as cross beds (arrow). Photo from 107.4 meters; mechanical pencil for scale. B) Shale beds immediately adjacent to beds with current structures have a shelly fauna, with evidence of transport, such as this cluster of trilobite cephalons. Photo from local float at 117 meters, mechanical pencil for scale. C) The lower half of the medial shale also contains laminated grey shale intervals, such as this photo spanning ~114-115 meters, at the 'waterfall quarry' level. 30 cm geological hammer for scale. These intervals host rare soft-bodied preservation. D) In-situ fragment of anomalocarid claw (arrow), from 114 meters (within 'waterfall quarry'); diameter of Canadian quarter is 24 mm. E) *Lingulosacculus nuda* (64) with preserved gut trace (arrow), from '*Lingulosacculus* quarry' at 118.2-118.6 meters. 5 mm scale bar on photo.

Figure 3- Lithostratigraphy and sedimentary geochemistry of the Mural Formation at Mumm Peak. Total measured thickness of the Formation is very similar to that of (59) but the heights of internal units differ slightly. *Nevadella-Bonnia/Olenellus* boundary is resolved to a 3.85m interval between 117.3m and 121.15m. Inset shows expanded stratigraphy of medial shale/siltstone. Geochemical data from left-to-right: 1) The iron speciation proxy (FeHR/FeT). Values above the vertical 0.38 line likely represent deposition under an anoxic water column, based on calibrations from the modern ocean (25). Oxic samples in the modern fall below this line, but anoxic samples can too, for instance during turbiditic sedimentation. The dashed 0.2 line represents the lowest modern value for an anoxic turbiditic sediment. FeP/FeHR values not graphed as all samples show an oxic signature; the average is 0.29 ± 0.15 (Supplemental Information) (27). 2) Fe/Al ratio, with shaded blue bar representing the range of values seen in ancient oxic shale (72). Values above this bar would indicate iron enrichment due to an anoxic water column. 3) Molybdenum Enrichment Factor (EF). 4) Uranium EF. 5) Vanadium EF. For these samples, an Enrichment Factor of 1 represents an aluminum-normalized value equal to upper continental crust (30). Values above 1 indicate enrichment, although recognition of muted enrichments can be difficult due to variations in detrital input (41). Enrichment would be expected under an anoxic water column (28), yet all of these samples are unenriched. McNton. = McNaughton Formation; W. = 'waterfall quarry' level from 112.8-114.9m; L. = '*Lingulosacculus* quarry' from 118.2-118.6m.

References

1. Erwin DH, Laflamme M, Tweedt SM, Sperling EA, Pisani D, Peterson KJ. The Cambrian conundrum: Early divergence and later ecological success in the early history of animals. Science. 2011;334(6059):1091–7.

2. Droser ML, Gehling JG, Jensen S. When the worm turned: Concordance of Early Cambrian ichnofabric and trace-fossil record in siliclastic rocks of South Australia. Geology. 1999;27:625–8.

3. Droser ML, Bottjer DJ. Trends in depth and extent of bioturbation in Cambrian carbonate marine environments, western United States. Geology. 1988;16:233–6.

4. Buatois LA, Mángano MG, Olea RA, Wilson MA. Decoupled evolution of soft and hard substrate communities during the Cambrian Explosion and Great Ordovician Biodiversification Event. Proc Natl Acad Sci. 2016 Jun 21;113(25):6945–8.

5. Porter SM. Closing the phosphatization window: Testing for the influence of taphonomic megabias on the pattern of small shelly fossil decline. Palaios. 2004;19:178–83.

6. Smith EF, Macdonald FA, Petach TA, Bold U, Schrag DP. Integrated stratigraphic, geochemical, and paleontological late Ediacaran to early Cambrian records from southwestern Mongolia. GSA Bull. 2016 Mar 1;128(3–4):442–68.

7. Maloof AC, Porter SM, Moore JL, Dudas FO, Bowring SA, Higgins JA, et al. The earliest Cambrian record of animals and ocean geochemical change. Geol Soc Am Bull. 2010;122:1731–74.

8. Butterfield N, Harvey T. Small carbonaceous fossils (SCFs): A new measure of early Paleozoic paleobiology. Geology. 2012;40(1):71–4.

9. Harvey THP, Vélez MI, Butterfield NJ. Exceptionally preserved crustaceans from western Canada reveal a cryptic Cambrian radiation. Proc Natl Acad Sci. 2012;109(5):1589–94.

10. Gaines RR. Burgess Shale-type Preservation and its Distribution in Space and Time. Paleontol Soc Pap. 2014 Oct;20:123–46.

11. Sperling EA. Tackling the 99%: can we begin to understand the paleoecology of the small and soft-bodied animal majority? In: Bush AM, Pruss SB, Payne JL, editors. Ecosystem paleobiology and geobiology. 2013. p. 77–86.

12. Conway Morris SC. The community structure of the Middle Cambrian Phyllopod Bed (Burgess Shale). Palaeontology. 1986;29:427–67.

13. Briggs DEG. Extraordinary fossils reveal the nature of Cambrian life: a commentary on Whittington (1975) ‘The enigmatic animal Opabinia regalis, Middle Cambrian, Burgess Shale, British Columbia.’ Phil Trans R Soc B. 2015 Apr 19;370(1666):20140313.

14. Briggs DEG. Extraordinary Fossils. Am Sci. 1991;79(2):130–41.

15. Caron J-B, Jackson DA. Paleoecology of the Greater Phyllopod Bed community, Burgess Shale. Palaeogeogr Palaeoclimatol Palaeoecol. 2008 Feb 18;258(3):222–56.

16. Briggs DEG, Fortey RA. Wonderful strife: systematics, stem groups, and the phylogenetic signal of the Cambrian radiation. Paleobiology. 2005;31 Supplement:94–112.

17. Allison PA, Briggs DEG. Exceptional fossil record: Distribution of soft-tissue preservation through the Phanerozoic. Geology. 1993 Jun 1;21(6):527–30.

18. Muscente AD, Schiffbauer JD, Broce J, Laflamme M, O'Donnell K, Boag TH, et al. Exceptionally preserved fossil assemblages through geologic time and space. Gondwana Res. 2017 Aug 1;48:164–88.

19. Allison PA. The Role of anoxia in the decay and mineralization of proteinaceous macro-fossils. Paleobiology. 1988 Jan 1;14:139–54.

20. Hammarlund E, Canfield DE, Bengtson S, Leth PM, Schillinger B, Calzada E. The influence of sulfate concentration on soft-tissue decay and preservation. Palaeontogr Can. 2011;(31):141–56.

21. Skinner ES. Taphonomy and depositional circumstances of exceptionally preserved fossils from the Kinzers Formation (Cambrian), southeastern Pennsylvania. Palaeogeogr Palaeoclimatol Palaeoecol. 2005;220(1–2):167–92.

22. Briggs DEG. The role of decay and mineralization in the preservation of soft-bodied fossils. Annu Rev Earth Planet Sci. 2003;31:275–301.

23. Naimark E, Kalinina M, Boeva N. PERSISTENCE OF EXTERNAL ANATOMY OF SMALL CRUSTACEANS IN A LONG TERM TAPHONOMIC EXPERIMENT. PALAIOS. 2018 Apr 10;33(4):154–63.

24. Gaines RR, Droser ML. The paleoredox setting of Burgess Shale-type deposits. Palaeogeogr Palaeoclimatol Palaeoecol. 2010 Nov 20;297(3):649–61.

25. Raiswell R, Canfield DE. Sources of iron for pyrite formation in marine sediments. Am J Sci. 1998;298:219–45.

26. Poulton SW, Canfield DE. Ferruginous conditions: A dominant feature of the ocean through Earth's history. Elements. 2011;7(2):107–12.

27. Sperling EA, Carbone C, Strauss JV, Johnston DT, Narbonne GM, Macdonald FA. Oxygen, facies, and secular controls on the appearance of Cryogenian and Ediacaran body and trace fossils in the Mackenzie Mountains of northwestern Canada. Geol Soc Am Bull. 2016;128:558–75.

28. Tribovillard N, Algeo TJ, Lyons T, Riboulleau A. Trace metals as paleoredox and paleoproductivity proxies: An update. Chem Geol. 2006;232(1):12–32.

29. Turekian KK, Wedepohl KH. Distribution of the elements in some major units of the earth's crust. Geol Soc Am Bull. 1961;72(2):175–92.

30. McLennan SM. Relationships between the trace element composition of sedimentary rocks and upper continental crust. Geochem Geophys Geosystems. 2001 Apr 1;2(4):1021.

31. Helz GR, Miller CV, Charnock JM, Mosselmans JFW, Pattrick RAD, Garner CD, et al. Mechanism of molybdenum removal from the sea and its concentration in black shales: EXAFS evidence. Geochim Cosmochim Acta. 1996 Oct 1;60(19):3631–42.

32. Erickson BE, Helz GR. Molybdenum(VI) speciation in sulfidic waters:. Stability and lability of thiomolybdates. Geochim Cosmochim Acta. 2000 Apr 1;64:1149–58.

33. Wanty RB, Goldhaber MB. Thermodynamics and kinetics of reactions involving vanadium in natural systems: Accumulation of vanadium in sedimentary rocks. Geochim Cosmochim Acta. 1992 Apr 1;56(4):1471–83.

34. Guilbaud R, Poulton SW, Butterfield NJ, Zhu M, Shields-Zhou GA. A global transition to ferruginous conditions in the early Neoproterozoic oceans. Nat Geosci. 2015;8:466–70.

35. Sperling EA, Wolock CJ, Morgan AS, Gill BC, Kunzmann M, Halverson GP, et al. Statistical analysis of iron geochemical data suggests limited late Proterozoic oxygenation. Nature. 2015 Jul 22;523(7561):451–4.

36. Canfield DE, Poulton SW, Knoll AH, Narbonne GM, Ross G, Goldberg T, et al. Ferruginous conditions dominated later Neoproterozoic deep-water chemistry. Science. 2008;321:949–52.

37. Sperling EA, Rooney AD, Hays L, Sergeev VN, Vorob'eva NG, Sergeeva ND, et al. Redox heterogeneity of subsurface waters in the Mesoproterozoic ocean. Geobiology. 2014;12:373–386.

38. Li C, Planavsky NJ, Love GD, Reinhard CT, Hardisty D, Feng L, et al. Marine redox conditions in the middle Proterozoic ocean and isotopic constraints on authigenic carbonate formation: Insights from the Chuanlinggou Formation, Yanshan Basin, North China. Geochim Cosmochim Acta. 2015 Feb 1;150:90–105.

39. Marz C, Poulton SW, Beckmann B, Kuster K, Wagner T, Kasten S. Redox sensitivity of P cycling during marine black shale formation: Dynamics of sulfidic and anoxic, non-sulfidic bottom waters. Geochim Cosmochim Acta. 2008;72:3703–17.

40. Miller AJ, Strauss JV, Halverson GP, MacDonald FA, Johnston DT, Sperling EA. Tracking the onset of Phanerozoic-style redox-sensitive trace metal enrichments: New results from basal Ediacaran post-glacial strata in NW Canada. Chem Geol. 2017 Mar 1;457:24–37.

41. Cole DB, Zhang S, Planavsky NJ. A new estimate of detrital redox-sensitive metal concentrations and variability in fluxes to marine sediments. Geochim Cosmochim Acta. 2017 Oct 15;215:337–53.

42. Raiswell R, Canfield DE. The iron biogeochemical cycle past and present. Geochem Perspect. 2012;1(1):1–322.

43. Hammarlund EU, Gaines RR, Prokopenko MG, Qi C, Hou X-G, Canfield DE. Early Cambrian oxygen minimum zone-like conditions at Chengjiang. Earth Planet Sci Lett. 2017 Oct 1;475:160–8.

44. Kloss TJ, Dornbos SQ, Chen J-Y, McHenry LJ, Marenco PJ. High-resolution geochemical evidence for oxic bottom waters in three Cambrian Burgess Shale-type deposits. Palaeogeogr Palaeoclimatol Palaeoecol. 2015 Dec 15;440:90–5.

45. Hammarlund E, Smith, M.P., Rasmussen, J., Nielsen, A., Canfield, D., Harper, D. The Sirius Passet Lagerstätte of North Greenland - a geochemical window on early Cambrian low oxygen environments and ecosystems. Geobiology. in review;

46. Powell WG, Johnston PA, Collom CJ. Geochemical evidence for oxygenated bottom waters during deposition of fossiliferous strata of the Burgess Shale Formation. Palaeogeogr Palaeoclimatol Palaeoecol. 2003 Dec 5;201(3):249–68.

47. Boudec AL, Ineson J, Rosing M, Døssing L, Martineau F, Lécuyer C, et al. Geochemistry of the Cambrian Sirius Passet Lagerstätte, Northern Greenland. Geochem Geophys Geosystems. 2014 Apr 1;15(4):886–904.

48. McKirdy DM, Hall PA, Nedin C, Halverson GP, Michaelsen BH, Jago JB, et al. Paleoredox status and thermal alteration of the lower Cambrian (Series 2) Emu Bay Shale Lagerstätte, South Australia. Aust J Earth Sci. 2011 Apr 1;58(3):259–72.

49. Kimmig J, Pratt BR. Taphonomy of the middle Cambrian (Drumian) Ravens Throat River Lagerstätte, Rockslide Formation, Mackenzie Mountains, Northwest Territories, Canada. Lethaia. 2016 Apr 1;49(2):150–69.

50. Novek JM, Dornbos SQ, McHenry LJ. Palaeoredox geochemistry and bioturbation levels of the exceptionally preserved early Cambrian Indian Springs biota, Nevada, USA. Lethaia. 2016 Oct 1;49(4):604–16.

51. Jones B, Manning DAC. Comparison of geochemical indices used for the interpretation of palaeoredox conditions in ancient mudstones. Chem Geol. 1994;111:111–29.

52. Pope MC, Hollingsworth JS, Dilliard K. Overview of Lower Cambrian mixed carbonate-siliciclastic deposition along the western Laurentian passive margin. In: Derby JR, Fritz RD, Longacre SA, Morgan WA, Sternbach CA, editors. The great American carbonate bank: The geology and economic resources of the Cambrian-Ordovician Suak megasequence of Laurentia. AAPG Memoir; 2012. p. 735–50.

53. Pyle LJ. Cambrian and Lower Ordovician Sauk megasequence of northwestern Canada, northern Rocky Mountains to the Beaufort Sea. In: Derby JR, Fritz RD, Longacre SA, Morgan WA, Stembach CA, editors. The great American carbonate bank: The geology and

economic resources of the Cambrian-Ordovician Sauk megasequence of Laurentia. 2012. p. 675–723.

54. Slind OL, Perkins GD. Lower Paleozoic and Proterozoic sediments of the Rocky Mountains between Jasper, Alberta and Pine River, British Columbia. Bull Can Pet Geol. 1966;14(4):442–68.

55. McMechan ME. Upper Proterozoic to Middle Cambrian history of the Peace River Arch: evidence from the Rocky Mountains. Bull Can Pet Geol. 1990;38(1):36–44.

56. Bond GC, Christie-Blick N, Kominz MA, Devlin WJ. An early Cambrian rift to post-rift transition in the Cordillera of western North America. Nature. 1985;315:742–6.

57. Lickorish WH, Simony PS. Evidence for late rifting of the Cordilleran margin outlined by stratigraphic division of the Lower Cambrian Gog Group, Rocky Mountain Main Ranges, British Columbia and Alberta. Can J Earth Sci. 1995 Jul 1;32(7):860–74.

58. Fritz WH. Walcott's lower Cambrian olenellid trilobite collection 61K, Mount Robson area, Canadian Rocky Mountains /. Ottawa, Canada : Geological Survey of Canada,; 1992.

59. Fritz WH, Mountjoy EW. Lower and early Middle Cambrian formations near Mount Robson, British Columbia and Alberta. Can J Earth Sci. 1975;12(2):119–31.

60. Walcott CD. New Lower Cambrian subfauna. Smithson Misc Collect. 1913;57:309–26.

61. Balthasar U. Mummpikia Gen. Nov. and the origin of calcitic-shelled brachiopods. Palaeontology. 2008;51:263–79.

62. Balthasar U. Shell structure, ontogeny and affinities of the Lower Cambrian bivalved problematic fossil Mickwitzia muralensis. Lethaia. 2004;37:381–400.

63. Ortega-Hernández J, Esteve J, Butterfield NJ. Humble origins for a successful strategy: complete enrolment in early Cambrian olenellid trilobites. Biol Lett. 2013 Oct 23;9(5):20130679.

64. Balthasar U, Butterfield NJ. Early Cambrian "soft-shelled" brachiopods as possible stem-group phoronids. Acta Palaeontol Pol. 2009;54:307–14.

65. Canfield DE, Raiswell R, Westrich JT, Reaves CM, Berner RA. The use of chromium reduction in the analysis of reduced inorganic sulfur in sediments and shale. Chem Geol. 1986;54:149–55.

66. Poulton SW, Canfield DE. Development of a sequential extraction procedure for iron: implications for iron partitioning in continentally derived particulates. Chem Geol. 2005;214:209–21.

67. Anbar AD, Duan Y, Lyons TW, Arnold GL, Kendall B, Creaser RA, et al. A whiff of oxygen before the Great Oxidation Event? Science. 2007;317:1903–6.

650 68. Read PB, Woodsworth GJ, Greenwood HJ, Ghent ED, Evenchick CA. Metamorphic map of
651 the Canadian Cordillera. “A” Series Map 1714A. Geological Survey of Canada; 1991.

652 69. Diamond CW, Planavsky NJ, Wang C, Lyons, TW. What the ~1.4 Ga Xiamaling Formation
653 can and cannot tell us about the mid-Proterozoic ocean. Geobiology. 2018;16:219–36.

654 70. Slotznick SP, Eiler JM, Fischer WW. The effects of metamorphism on iron mineralogy and
655 the iron speciation redox proxy. Geochim Cosmochim Acta. 2018 Mar 1;224:96–115.

656 71. Lyons TW, Severmann S. A critical look at iron paleoredox proxies: New insights from
657 modern euxinic marine basins. Geochim Cosmochim Acta. 2006;70:5698–722.

658 72. Raiswell R, Newton R, Bottrell SH, Coburn PM, Briggs DEG, Bond DPG, et al. Turbidite
659 depositional influences on the diagenesis of Beecher’s Trilobite Bed and the Hunsrück Slate;
660 sites of soft tissue pyritization. Am J Sci. 2008;308(2):105–29.

661 73. Paterson JR, García-Bellido DC, Lee MSY, Brock GA, Jago JB, Edgecombe GD. Acute
662 vision in the giant Cambrian predator *Anomalocaris* and the origin of compound eyes.
663 Nature. 2011 Dec;480(7376):237–40.

664 74. Ma X, Cong P, Hou X, Edgecombe GD, Strausfeld NJ. An exceptionally preserved
665 arthropod cardiovascular system from the early Cambrian. Nat Commun. 2014 Apr 7;5:3560.

666 75. Ma X, Hou X, Edgecombe GD, Strausfeld NJ. Complex brain and optic lobes in an early
667 Cambrian arthropod. Nature. 2012 Oct;490(7419):258–61.

668 76. Butterfield NJ. Leanchoilia guts and the interpretation of three-dimensional structures in
669 Burgess Shale-type fossils. Paleobiology. 2002;28(1):155–71.

670 77. Boyer DL, Owens JD, Lyons TW, Droser ML. Joining Forces: Combined Biological and
671 Geochemical Proxies Reveal A Complex but Refined High-Resolution Palaeo-oxygen
672 History in Devonian Epeiric Seas. Palaeogeogr Palaeoclimatol Palaeoecol. 2011;306:134–
673 146.

674 78. Gaines RR, Droser ML. Paleoecology of the familiar trilobite Elrathia kingii: An early
675 exaerobic zone inhabitant. Geology. 2003;31:941–4.

676 79. Garson DE, Gaines RR, Droser ML, Liddell WD, Sappenfield A. Dynamic palaeoredox and
677 exceptional preservation in the Cambrian Spence Shale of Utah. Lethaia. 2011;

678 80. Ahm A-SC, Bjerrum CJ, Hammarlund EU. Disentangling the record of diagenesis, local
679 redox conditions, and global seawater chemistry during the latest Ordovician glaciation.
680 Earth Planet Sci Lett. 2017 Feb 1;459:145–56.

681 81. Scott C, Lyons TW. Contrasting molybdenum cycling and isotopic properties in euxinic
682 versus non-euxinic sediments and sedimentary rocks: refining the paleoproxies. Chem Geol.
683 2012;324:19–27.

82. Dahl TW, Ruhl M, Hammarlund EU, Canfield DE, Rosing MT, Bjerrum CJ. Tracing euxinia by molybdenum concentrations in sediments using handheld X-ray fluorescence spectroscopy (HHXRF). Chem Geol. 2013;360:241–51.

83. Gaines RR, Hammarlund EU, Hou X, Qi C, Gabbott SE, Zhao Y, et al. Mechanism for Burgess Shale-type preservation. Proc Natl Acad Sci. 2012;109(14):5180–4.

84. Bergmann KD, Grotzinger JP, Fischer WW. Biological influences on seafloor carbonate precipitation. PALAIOS. 2013 Feb 1;28(2):99–115.

85. Anderson RP, Tosca NJ, Gaines RR, Koch NM, Briggs DEG. A mineralogical signature for Burgess Shale–type fossilization. Geology. 2018;

86. Petrovich R. Mechanisms of Fossilization of the Soft-Bodied and Lightly Armored Faunas of the Burgess Shale and of Some Other Classical Localities. Am J Sci. 2001 Oct 1;301(8):683–726.

87. Wilson LA, Butterfield NJ. Sediment effects on the preservation of Burgess shale–type compression fossils. PALAIOS. 2014 Apr 1;29(4):145–54.

88. McMahon S, Anderson RP, Saupe EE, Briggs DEG. Experimental evidence that clay inhibits bacterial decomposers: Implications for preservation of organic fossils. Geology. 2016;44:867–70.

89. Canfield DE. Reactive iron in marine sediments. Geochim Cosmochim Acta. 1989;53(3):619–32.

90. Lyons TW, Reinhard CT, Planavsky NJ. The rise of oxygen in Earth's early ocean and atmosphere. Nature. 2014;506(7488):307–15.

91. Canfield DE, Farquhar J. Animal evolution, bioturbation, and the sulfate evolution of the oceans. Proc Natl Acad Sci USA. 2009;106:8123–7.

92. Lyons TW. A perfect (geochemical) storm yielded exceptional fossils in the early ocean. Proc Natl Acad Sci. 2012 Apr 3;109(14):5138–9.

93. Montjoy EW. Geology, Mount Robson, West of Sixth Meridian, Alberta-British Columbia. Geological Survey of Canada; 1980. ("A" Map Series Map 1499A).

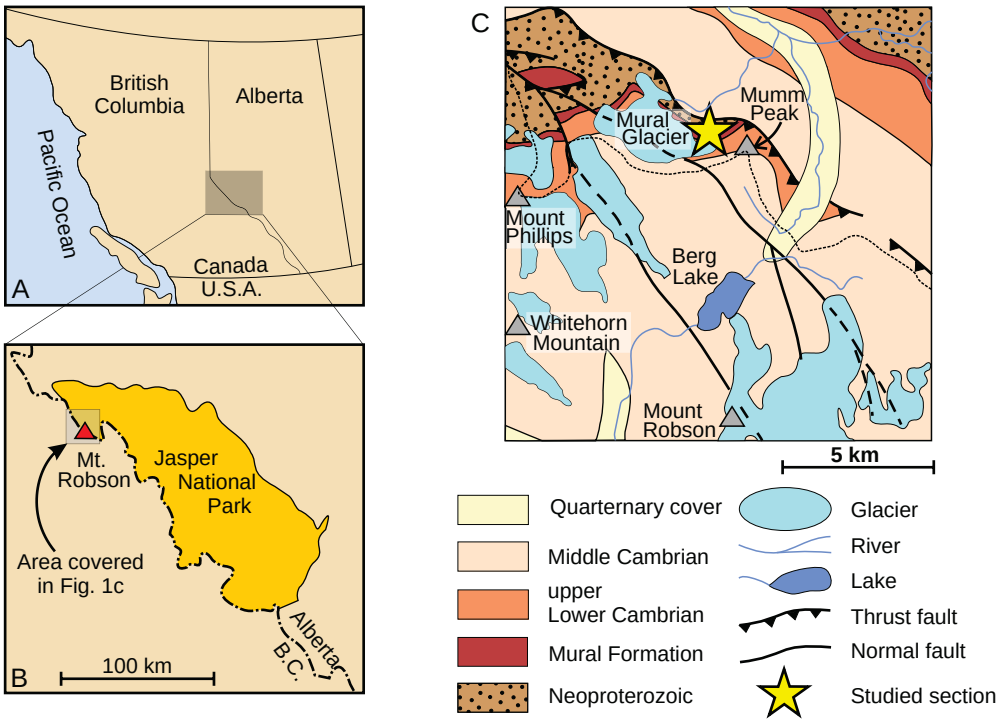
A
British Columbia
Alberta
Pacific Ocean
Canada
U.S.A.
B
Mt. Robson
Jasper National Park
Area covered in Fig. 1c
Alberta
B.C.
100 km
C
Mumm Peak
Mural Glacier
Mount Phillips
Berg Lake
Whitehorn Mountain
Mount Robson
5 km
Quarternary cover
Middle Cambrian
upper Lower Cambrian
Mural Formation
Neoproterozoic
Glacier
River
Lake
Thrust fault
Normal fault
Studied section


A.


B.

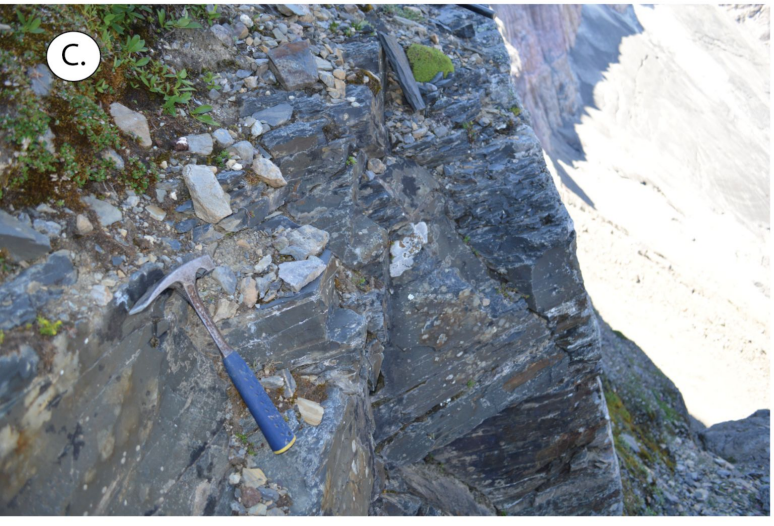
C.

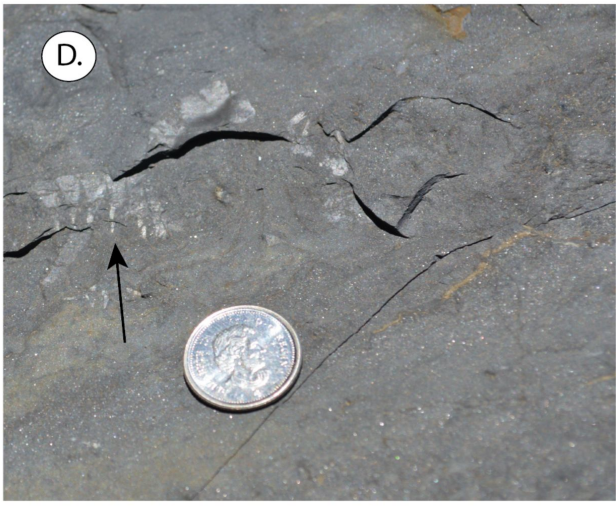
D.

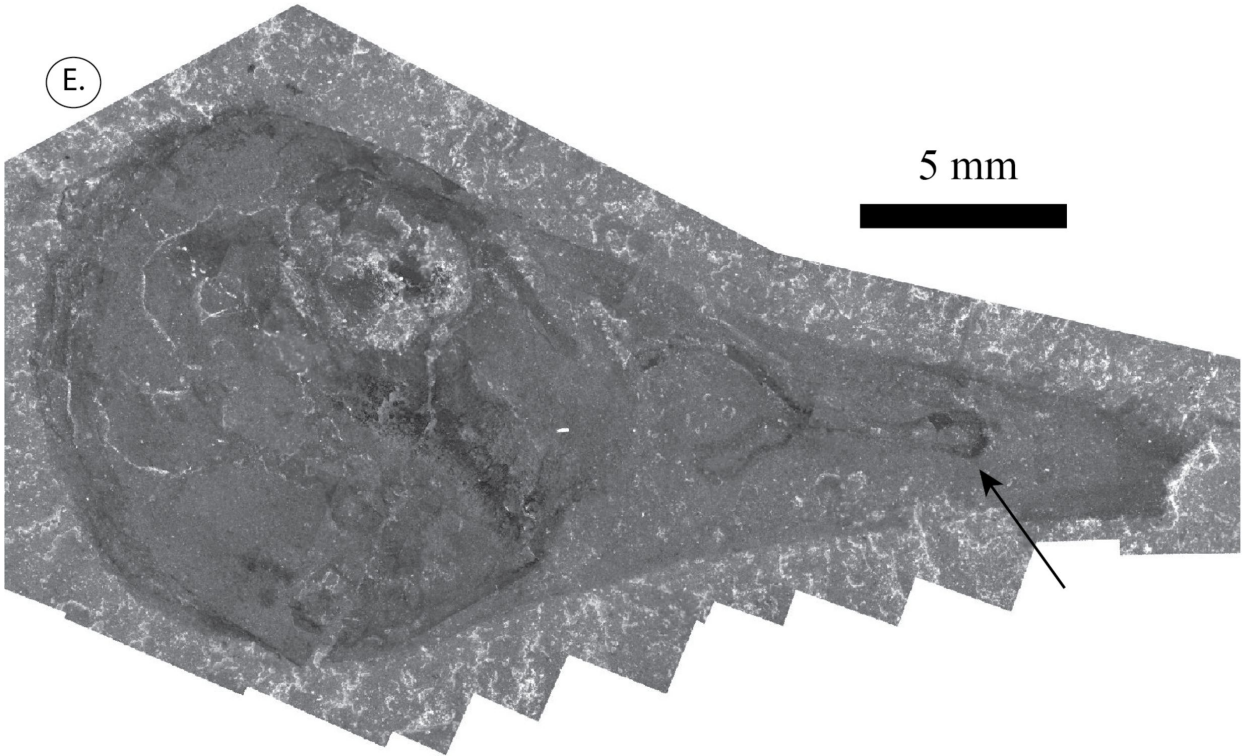
E.
5 mm

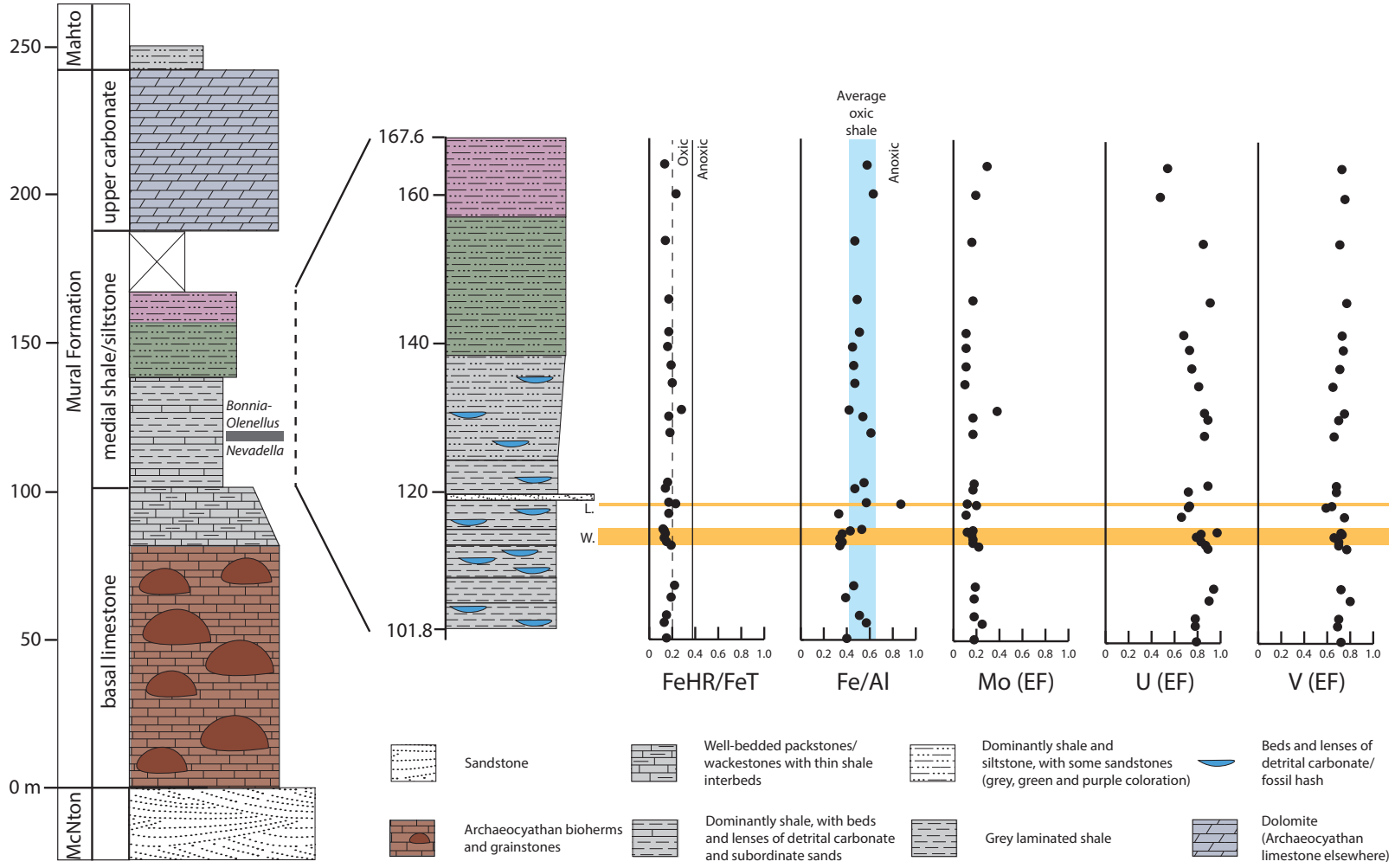
Mahto
Mural Formation
upper carbonate
medial shale/siltstone
basal limestone
McNton
250
200
150
100
50
0 m
Bonnia-
Olenellus
Nevadella
167.6
160
140
120
101.8
L.
W.
Average
oxic
shale
Oxic
Anoxic
Anoxic
0 0.2 0.4 0.6 0.8 1.0
FeHR/FeT
Fe/Al
Mo (EF)
U (EF)
V (EF)
Sandstone
Well-bedded packstones/
wackestones with thin shale
interbeds
Dominantly shale and
siltstone, with some sandstones
(grey, green and purple coloration)
Beds and lenses of
detrital carbonate/
fossil hash
Archaeocyathan bioherms
and grainstones
Dominantly shale, with beds
and lenses of detrital carbonate
and subordinate sands
Grey laminated shale
Dolomite
(Archaeocyathan
limestone elsewhere)

SGP sample_i	Original_num	Height_in_se	Lithology	Fe-carb (wt%	Fe-ox (wt%)	Fe-mag (wt%
3321	S1409-100.2	100.2	shale	0.188	0.176	0.122
3322	S1409-102.3	102.3	shale	0.267	0.144	0.145
3323	S1409-103.3	103.3	shale	0.177	0.218	0.186
3324	S1409-105.7	105.7	shale	0.127	0.225	0.097
3325	S1409-107.3	107.3	shale	0.148	0.421	0.165
3326	S1409-112.7	112.7	shale	0.138	0.218	0.098
3327	S1409-113.2	113.2	shale	0.112	0.108	0.123
3328	S1409-113.7	113.7	shale	0.113	0.053	0.151
3329	S1409-114.3	114.3	shale	0.108	0.097	0.173
3330	S1409-114.7	114.7	shale	0.144	0.085	0.18
3331	S1409-114.9	114.9	shale	0.161	0.073	0.179
3332	S1409-117	117	shale	0.102	0.115	0.077
3333	S1409-118.3	118.3	shale	0.241	0.476	0.375
3334	S1409-118.5	118.5	shale	0.21	0.161	0.298
3335	S1409-120.4	120.4	shale	0.166	0.042	0.187
3336	S1409-121.2	121.2	shale	0.248	0.058	0.195
3337	S1409-127.9	127.9	shale	0.499	0.078	0.27
3338	S1409-130.1	130.1	shale	0.339	0.08	0.218
3339	S1409-131	131	shale	0.214	0.174	0.15
3340	S1409-134.6	134.6	shale	0.245	0.095	0.186
3341	S1409-137	137	shale	0.183	0.041	0.156
3342	S1409-139.5	139.5	shale	0.238	0.054	0.224
3343	S1409-141.5	141.5	shale	0.313	0.06	0.277
3344	S1409-145.9	145.9	shale	0.125	0.344	0.237
3345	S1409-153.8	153.8	shale	0.14	0.097	0.16
3346	S1409-160.1	160.1	shale	0.143	0.964	0.218
3347	S1409-164	164	shale	0.117	0.461	0.129
			Average	0.19	0.19	0.18
			Standard Dev	0.09	0.20	0.07

Fe-py (wt%)	FeT (wt%)	FeHR	FeHR/FeT	Fe-py/FeHR	FeT/Al	TOC (wt%)
0.079	3.82	0.57	0.15	0.14	0.4	0.13
0.089	4.87	0.65	0.13	0.14	0.57	0.13
0.109	4.51	0.69	0.15	0.16	0.51	0.15
0.232	3.5	0.68	0.19	0.34	0.39	0.12
0.128	3.94	0.86	0.22	0.15	0.46	0.18
0.189	3.32	0.64	0.19	0.3	0.34	0.19
0.238	4.03	0.58	0.15	0.41	0.36	0.16
0.185	3.95	0.51	0.13	0.37	0.34	0.16
0.166	4.22	0.55	0.14	0.31	0.36	0.16
0.182	4.54	0.59	0.13	0.31	0.43	0.19
0.216	5.67	0.63	0.12	0.35	0.53	0.22
0.272	3.24	0.56	0.17	0.48	0.33	0.18
0.514	7.46	1.6	0.23	0.32	0.87	0.15
0.284	5.83	0.95	0.17	0.3	0.57	0.13
0.219	4.45	0.62	0.14	0.36	0.47	0.14
0.276	4.97	0.78	0.16	0.36	0.55	0.15
0.185	5.66	1.04	0.18	0.18	0.61	0.13
0.2	5.02	0.84	0.17	0.24	0.54	0.15
0.648	4.22	1.19	0.28	0.55	0.42	0.14
0.47	4.87	1	0.2	0.47	0.47	0.11
0.465	4.58	0.85	0.19	0.55	0.46	0.15
0.211	4.43	0.73	0.16	0.29	0.45	0.12
0.196	4.92	0.85	0.17	0.24	0.51	0.09
0.057	4.63	0.77	0.17	0.08	0.49	0.12
0.234	4.59	0.63	0.14	0.37	0.47	0.1
0.006	5.91	1.34	0.23	0.01	0.62	0.12
0.012	5.43	0.72	0.13	0.01	0.57	0.1
0.22	4.69	0.79	0.17	0.29	0.48	0.14
0.15	0.91	0.26	0.04	0.15	0.11	0.03

Al (wt%)	Ca (wt%)	K (wt%)	Mg (wt%)	Mn (ppm)	Mo (ppm)	Mo EF
9.08	1.27	4.37	1.36	245	0.3	0.18
8.48	4.11	3.8	1.38	629	0.4	0.25
8.85	0.77	4.18	1.36	246	0.3	0.18
8.96	0.09	4.92	0.97	82	0.3	0.18
8.52	0.11	4.16	1.05	105	0.3	0.19
9.64	0.09	5.42	0.81	104	0.4	0.22
9.21	0.07	4.91	1	167	0.3	0.17
9.71	0.14	4.67	1.05	195	0.3	0.17
9.84	0.26	4.66	1.12	255	0.3	0.16
9	0.34	5.13	1.12	265	0.2	0.12
9.2	0.09	4.59	1.21	241	0.3	0.17
9.96	0.07	5.68	0.82	106	0.2	0.11
8	0.47	2.57	1.86	703	0.3	0.2
8.99	0.44	3.42	1.48	479	0.2	0.12
9.51	0.27	4.39	1.09	276	0.3	0.17
9.03	0.4	4.1	1.2	539	0.3	0.18
9.33	0.72	3.92	1.45	1120	0.3	0.17
9.38	0.41	4.45	1.25	911	0.3	0.17
9.97	0.3	5.2	0.86	737	0.7	0.38
10.3	0.3	5.07	1.11	726	0.2	0.1
9.9	0.08	4.82	1.19	556	0.2	0.11
9.89	0.06	4.73	1.14	888	0.2	0.11
9.74	0.15	4.44	1.18	1256	0.2	0.11
9.42	0.08	3.94	0.98	588	0.3	0.17
9.83	0.04	4.23	1.02	266	0.3	0.16
9.55	0.08	2.62	1.16	1295	0.2	0.17
9.57	0.1	2.78	1.11	399	0.3	0.17
9.37	0.42	4.34	1.16	495.52	0.29	0.17
0.53	0.79	0.79	0.22	359.41	0.10	0.06

Na (wt%)	P (ppm)	Th (ppm)	Ti (wt%)	U (ppm)	U EF	V (ppm)
0.933	470	18.6	0.426	2.5	0.79	87
0.944	480	16.4	0.374	2.3	0.78	78
0.945	540	17.7	0.371	2.4	0.78	83
0.805	370	17.3	0.441	2.8	0.9	95
0.783	520	19	0.391	2.8	0.94	82
0.547	540	15.7	0.444	3	0.89	99
0.639	350	16.3	0.431	2.8	0.87	86
0.535	540	15.4	0.428	2.8	0.83	90
0.532	880	17.4	0.407	2.7	0.79	87
0.523	990	15.3	0.397	2.6	0.83	88
0.601	340	16.8	0.398	3.1	0.97	88
0.565	280	16.2	0.455	2.3	0.66	100
0.987	1430	15	0.309	2	0.72	63
0.89	1150	20.3	0.429	2.3	0.73	76
0.818	550	16.7	0.433	2.4	0.72	86
0.73	730	19.3	0.444	2.8	0.89	82
0.649	870	17.8	0.432	2.8	0.86	82
0.556	600	17.2	0.431	2.9	0.89	87
0.465	590	19.8	0.469	3	0.86	99
0.403	650	17.9	0.419	2.9	0.81	89
0.407	230	15.1	0.382	2.6	0.75	93
0.472	270	16.3	0.426	2.5	0.73	98
0.81	640	14.2	0.364	2.3	0.68	94
0.284	330	18.6	0.46	3	0.91	96
0.337	230	15	0.385	2.9	0.85	93
0.266	300	12.4	0.362	1.6	0.48	94
0.277	260	13.1	0.376	1.8	0.54	92
0.62	560.37	16.70	0.41	2.59	0.79	88.41
0.22	295.55	1.94	0.04	0.38	0.11	8.21

V EF	Zn (ppm)	Zr (ppm)
0.72	51	74.7
0.69	60	70.1
0.7	62	68.1
0.8	54	73
0.72	56	81.5
0.77	41	80.2
0.7	58	68.6
0.7	66	68.8
0.66	71	61.1
0.73	70	59.9
0.72	103	59.7
0.75	37	69.8
0.59	124	45.5
0.64	92	60.3
0.68	61	59.9
0.68	80	63.4
0.66	109	55.9
0.7	100	57
0.75	61	70.4
0.65	83	61.8
0.71	93	64.1
0.74	88	72.2
0.73	96	67.9
0.77	73	78.5
0.71	76	75.2
0.74	78	36.3
0.72	68	38.5
0.71	74.48	64.53
0.04	21.04	11.27